Journal of Structural Geology 33 (2011) 1764–1775

Contents lists available at SciVerse ScienceDirect

Journal of Structural Geology

journal homepage: www.elsevier.com/locate/jsg

Textures of syntaxial quartz veins synthesized by hydrothermal experiments

Atsushi Okamoto [a,*], Kotaro Sekine [b]

[a] Graduate School of Environmental Studies, Tohoku University, Aoba 6-6-20, Aramaki Aoba-ku, Sendai 980-8579, Japan
[b] Japan Oil Gas and Metals National Corporation, 1-2-2 Hamada, Mihama-ku, Chiba 261-0025, Japan

ARTICLE INFO

Article history:
Received 19 April 2011
Received in revised form
28 September 2011
Accepted 7 October 2011
Available online 14 October 2011

Keywords:
Quartz vein
Vein texture
Hydrothermal experiments
Competitive growth

ABSTRACT

Syntaxial quartz veins were synthesized by hydrothermal flow-through experiments using rock blocks (metachert, sandstone, and granite) containing slits. Based on analyses of vein textures using birefringence imaging microscopy, we identified two stages of crystal growth. During stage 1, quartz grain growth occurs without an increase in grain width. During stage 2, quartz grains develop facets and grow preferentially parallel to the *c*-axis orientation, and the aspect ratio of quartz grains shifts toward ~2.9. Competitive growth occurs significantly at stage 2, and the transition from stage 1–2 occurs at a critical distance from the vein wall, being approximately equal to the host-rock grain size. Crystal growth in the slits produce various textures controlled by the ratio of slit aperture (H) to host-rock grain size (d). In high H/d cracks, elongate–blocky texture develops by grain impingement during stage 2, whereas in low H/d cracks, crystals that bridge the crack form without competitive growth by grain impingement at stage 1. Heterogeneous structures of fracture porosity are produced during syntaxial vein formation, due to the anisotropy in the growth rate of quartz. Such "incompletely sealed" cracks may act as important fluid pathways and as weak planes in the upper crust.

1. Introduction

Quartz veins occur ubiquitously in mid- and upper-crustal rocks, suggesting that silica precipitation in cracks and faults influences spatial and temporal variations in the hydrological and mechanical properties of crustal rocks. Quartz veins show a variety of textures defined by the shape, size, and crystallographic orientation of grains in veins and their relation to the wall rock (e.g. Cox and Etheridge, 1983; Fisher and Brantley, 1992; Bons, 2000; Oliver and Bons, 2001; Hilgers and Urai, 2002a; Passchier and Trouw, 2005; Okamoto et al., 2008; Van Noten et al., 2011).

Bons (2000) identified four types of vein textures: fibrous, elongate–blocky, stretched crystal, and blocky. Fibrous veins are filled by extremely elongate grains that are commonly oriented perpendicular to the vein wall, and fiber width is constant in the growth direction (Hilgers and Urai, 2002a). Elongate–blocky veins are also filled by elongate grains, but with a moderate length/width ratio, usually less than 10 (Fisher and Brantley, 1992). The grain width increases in the growth direction. The growth of fibrous and elongate–blocky veins occurs at localized sites in veins in the following two ways: syntaxial vein growth that occurs inward from vein surfaces, and antitaxial vein growth that occurs outward from both sides of the vein (Bons, 2000).

Stretched crystal veins, which also contain elongate grains, form by repeated crack–sealing, with subsequent cracks cutting grains of the host rock and earlier vein-fillings at various sites (Bons, 2000; Okamoto et al., 2008; Becker et al., 2011). This type of vein growth is termed "ataxial", and is distinct from syntaxial and antitaxial growth. As a result of ataxial vein growth, grains in the wall rock bridge over the veins. These veins are characterized by serrated grain boundaries (e.g. Ramsay and Huber, 1987; Stowell et al., 1999). Blocky veins are filled by equant grains that are interpreted to form by continuous nucleation plus growth or secondary recrystallization in the veins (Oliver and Bons, 2001; Okamoto et al., 2008; Okamoto and Tsuchiya, 2009). In addition to the four textures described above, there exist composite veins, in which two or more of these textures occur together (e.g. Bons, 2000; Passchier and Trouw, 2005). Vein textures are expected to provide valuable clues to the nature of the earlier fluid-filled cracks, including information on fluid chemistry, fluid flow, material transport, and crack aperture during sealing. However, the interpretation and analysis of vein texture remains qualitative owing to the complicated mechanisms of vein formation, including fracturing, fluid transport, and mineral deposition.

An important phenomenon that distinguishes different vein types is competitive growth, by which grains with favorable

* Corresponding author. Tel./fax: +81 22 795 6336.
E-mail addresses: okamoto@mail.kankyo.tohoku.ac.jp (A. Okamoto), sekine-kotaro@jogmec.go.jp (K. Sekine).

0191-8141/$ – see front matter © 2011 Elsevier Ltd. All rights reserved.
doi:10.1016/j.jsg.2011.10.004

orientations and positions survive. Competitive growth occurs significantly during the formation of elongate–blocky veins, but not for fibrous and stretched crystal veins. The nature of competitive growth during vein formation has been studied with numerical simulations that use kinematic models of two-dimensional polycrystalline crystal growth (Urai et al., 1991; Bons, 2001; Hilgers et al., 2001; Zhang and Adams, 2002; Nollet et al., 2005; Gale et al., 2010). Hilgers et al. (2001) showed that antitaxial fibrous veins that lack competitive growth evolve when the ratio of crack-opening velocity to growth rate is low, and when vein wall roughness is high. Experimental studies of polycrystal growth from an advecting fluid onto a substrate have been carried out on calcite (Lee et al., 1996; Lee and Morse, 1999) and alum (Hilgers and Urai, 2002b; Hilgers et al., 2004; Nollet et al., 2006). In these experiments, distinct competitive growth occurred with the development of crystal facets.

However, it remains unclear whether the insights from numerical simulations and growth experiments of analog materials can be directly applied to the development of quartz veins. There have been few experimental studies on the formation of quartz veins, with some exceptions (Hilgers and Tenthorey, 2004; Okamoto et al., 2010). Based on hydrothermal flow-through experiments, Okamoto et al. (2010) showed that mineralogy in silica precipitates varies according to the degree of supersaturation and the presence of minor components in the solutions: metastable opal-A and opal-C formed predominantly from pure Si solutions, whereas quartz is the dominant precipitate from Si-supersaturated solutions with additional Al, Na, and K. Okamoto et al. (2010) reported that epitaxial growth occurred on pre-existing quartz grains; however, they did not observe competitive growth among adjacent grains because granite was used as the rock substrate.

Quartz veins with elongate–blocky and stretched crystal textures are commonly found within a single outcrop, and a composite texture, involving both texture types, is often found even in a single vein (Okamoto et al., 2008). The occurrence of such veins suggests that the difference between these textures is not controlled by temperature or the type of host rock; indeed, the controlling factor remains unknown.

In this study, we focus on the syntaxial growth of quartz from both walls in a crack (bitaxial growth). Bitaxial growth commonly occurs in the development of elongate–blocky veins. When the crystals on both sides of the vein wall have the same crystallographic orientation, growth from both walls can produce a crystal that bridges the vein and is optically continuous with crystals of the host rock (Laubach et al., 2004). In this paper, such a crystal is termed a “crystal bridge”. Stretched crystal veins are considered to develop via the repeated formation of crystal bridges at different sites in the vein (Bons, 2000). Therefore, an understanding of the nature of competitive growth and the formation of crystal bridges in a crack would aid in the interpretation of spatial variations in vein textures.

In this study, we synthesized syntaxial quartz veins by hydrothermal flow-through experiments. We observed the textures of polycrystal quartz growth in an open cavity, with a variety of host rocks (metachert, sandstone, granite). The grain size, aspect ratio, *c*-axis fabric, and shape preferred orientation of quartz grains in the veins were analyzed using a birefringence imaging microscope. The host rocks used in the experiments contain a slit, as an analog to an open crack. Based on the observations of polycrystal growth from both sides of the slit in the host rock and the results of a 2D crystal growth model, we describe the sealing processes with and without competitive growth and the formation of crystal bridges, and we discuss the implications of the findings in terms of the resulting vein textures. We also discuss the implications of the results regarding polycrystal growth in a slit for the evolution of fracture porosity during sealing of an open crack.

2. Synthesis of quartz veins

Syntaxial quartz veins were synthesized at 430 ± 1 °C and 31 ± 1 MPa by hydrothermal flow-through experiments. The experimental apparatus was the same as that used in Okamoto et al. (2010), except for the length of reaction vessels. To create a horizontal flow path, the system was composed of two stainless-steel (SUS316) tube-type reaction vessels with inner diameters of 10.8 mm. One vessel was used for the preparation of input solutions (R_0), and the second for precipitation (R_1) (Fig. 1a). The lengths of the R_0 and R_1 vessels were 510 and 320 mm, respectively. The fluid pressure (31 MPa) was regulated by a back-pressure valve. The respective temperatures of the R_0 and R_1 vessels were 360 ± 1 °C and 430 ± 1 °C. High-Si solutions were created in the R_0 vessel by dissolving mixtures of quartz sand (30 g, ~1 mm in diameter) and granite sand (Iidate granite from Japan, 30 g, ~1 mm in diameter). The input solutions were supersaturated with respect to quartz when reaching the R_1 vessel, because the solubility of quartz, $C_{Si,Qtz,eq}$, is much higher at 360 °C (450 ppm) than at 430 °C (98 ppm) (Fournier and Potter, 1982). The Iidate granite is composed of quartz, plagioclase, alkali feldspar, and biotite. The input solutions contained minor amounts of Al, Na, and K derived from feldspars in granite, which enhanced the precipitation of quartz and prevented the formation of metastable polymorphs, including opal-A and opal-C (Okamoto et al., 2010).

In the R_1 vessel, we set rock blocks with dimensions of approximately 5 × 5 × 20 mm as substrates. Five kinds of rock (three metacherts, one sandstone, and one granite) were used (Table 1). The host rocks had grain sizes ranging between 23 μm and 798 μm, and modal abundances of quartz, M_{Qtz}, were 0.98 in the metacherts, 0.52 and 0.32 in the sandstone and the granite, respectively. Each rock block had a slit with a 304–353 μm aperture that was 10–15 mm in length (Fig. 1b), made using a micro-cutter.

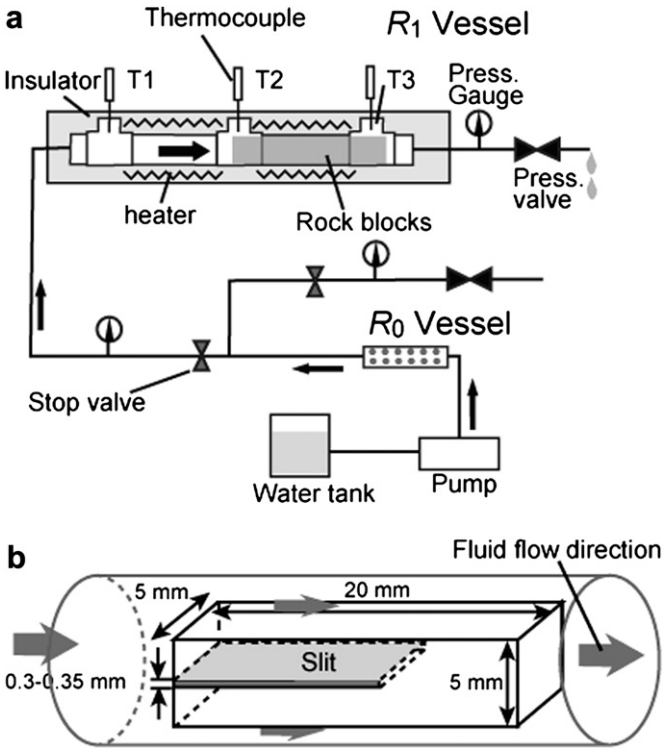

Fig. 1. Schematic illustrations of (a) the experimental apparatus used in flow-through experiments, and (b) the rock blocks within the R_1 vessel.

Table 1
Summary of condition for synthetizing quartz veins.

No.	Substrate rock type	d^a μm	M_{Qtz}	Other mineral	Slit width μm	Flow rate g/min	Duration h	Si ppm
JU3-2CH	Metachert from Mino-Tanba metamorphic belt	23	0.98	Ms	304	0.8	188	222–297
JU4-4IK	Metachert from the Ryoke metamorphic belt, Japan	140	0.98	Ms	340	1.2	336	147–205
JU4-5IH	Metachert from the Ryoke metamorphic belt, Japan	65	0.98	Ms	311	1.2	336	115–147
JU3-6SS	Sandstone from the Shimanto accretionary complex, Japan	80	0.52	Clay minerals	353	0.8	188	127–176
JU4-7Gr	Iidate granite from Japan	798	0.32	Pl, Kfs, Bt, Oq	348	1.2	336	100–103

[a] Average grain size of quartz of the host rock.

Rock blocks were set with the slit oriented horizontally, opening toward the upstream side.

Two runs were carried out, with a flow rate and duration of 0.8 g/min and 188 h for run 1, and 1.2 g/min and 320 h for run 2, respectively. In each run, we set five blocks in the downstream half of the R_1 vessel. During the experiments, input and output solutions were periodically sampled from the capillary tubes. The concentrations of Si and Al were determined using an inductively coupled plasma–atomic emission spectrometer (ICP–AES; Hitachi P-4000), while Na and K were determined by atomic absorption spectrometry (Varian AA240FS), both at Tohoku University, Japan. Following the experiments, the R_0 vessel was cut into several segments, and the reaction products and rock blocks were removed.

The chemistries of the input and output solutions were similar among the runs, and did not change significantly during individual runs. The Si content of the input solution, C_{Si}, was 330–367 ppm, corresponding to a supersaturation ratio, $C_{Si}/C_{Si,eq,Qtz}$, of ~3.5, which decreased to 101–112 ppm after passing through the R_1 vessel. The respective Al, Na, and K contents were 2.6, 3.8 and 1.8 ppm in the input solution, and <0.1, 1.5, and 0.2 ppm in the output solution. The time-averaged Si concentrations at intermediate vessel positions were obtained from C_{Si} values in the input and output solutions, and by the amount of precipitate at each vessel segment, following Okamoto et al. (2010).

Some rock blocks were broken when removed from the vessel because the precipitates caused them to stick tightly to the vessel wall. We selected five rock blocks (three metacherts, sandstone, and granite) for detailed observation (Table 1), preparing thin sections cut normal to the slit and parallel to the long axis of the blocks. For one metachert sample (JU4-5IH), only the outer surface of the block was observed in thin section cut parallel to the slit, because the slit was broken.

3. Method of texture analyses

The quantitative petrological observation of mineral spatial distribution and crystallographic orientation is known as AVA (*Achsenverteilungsanalyse* or axial distribution analysis; Sander, 1950). AVA images are commonly obtained with a computer-aided optical microscope by taking a series of thin section images while progressively rotating the polarizer and with a retardation plate inserted (Heilbronner and Pauli, 1993; Fueten and Goodchild, 2001; Wilson et al., 2007). This method has been applied to the textural analysis of quartz aggregates in deformed rocks (Heilbronner and Tullis, 2006) and in veins (Wilson et al., 2009). Based on the intensity variation observed in a quartz grain during rotation (e.g. the maximum intensity method suggested by Fueten and Goodchild, 2001), the *c*-axis orientation of a quartz grain in section is determined.

In the present study, textures of synthetic quartz veins were examined with an AVA imaging system: the Abrio® birefringence imaging microscope manufactured by Cambridge Research & Instrumentation. For a detailed explanation of this system, see Shribak and Oldenbourg (2003). The Abrio imaging system captures between two and five thin-section images under various conditions of circular polarized illumination. Liquid-crystal universal compensators are used for the illumination instead of the mechanical polarization controllers used in other AVA imaging systems. In subsequent image processing, the intensity of transmitted light through the optical train, including the thin section, is derived using Jones calculus. The system performs high-precision imaging in less than 10 s with unique algorithms, providing the two-dimensional distribution of retardance and the slow-axis orientation of birefringent materials. Retardance values range from 0 to 255, and the slow-axis orientation is given as the angle between the slow axis and a fixed reference direction, ranging from 0 to 180° in 1° increments. This imaging system has also been applied to photoelasticity analysis (Sekine et al., 2011).

For quartz, the azimuth of the *c*-axis, θ, is equal to the projection of the slow-axis orientation onto the thin section plane (Fig. 2a). In the present study, $\theta = 90°$ when the projection of the *c*-axis on the thin section plane is oriented normal to the vein wall. When the section thickness, h, is given, the plunge of the *c*-axis, ϕ (in radians), defined as the angle between the *c*-axis and the thin section normal (Fig. 2a), is derived from retardance as follows:

$$\phi = \cos^{-1}\left(n_0^2 n_e^2 \left(\frac{1}{\left(\frac{retardance}{h} + n_0 \right)^2} - \frac{1}{n_e^2} \right) \Big/ \left(n_e^2 - n_0^2 \right) \right)^{1/2} \quad (1)$$

where n_o and n_e are the refractive indices of ordinary and extraordinary light, which for quartz have respective values of 1.546 and 1.555.

The size of each image pixel was 2.47 μm, and each image comprised 1392 × 1024 pixels. We combined several images for vein analysis. It is difficult to know the exact thickness of the thin section. We assumed the *c*-axis of quartz grains with maximal retardation values was oriented normal to the plane of the thin section. This assumption is reasonable for the analyzed samples because the *c*-axis fabric of the host rocks shows a nearly random distribution, as shown below. Fig. 2b and c show the two-dimensional distributions of the azimuth (i.e., the projection of the slow-axis orientation onto the thin section plane), θ, and the plunge (i.e., the angle between the *c*-axis and the thin section normal), ϕ, of quartz grains in a metachert block used in a hydrothermal experiment (JU3-2CH). This metachert sample was collected from the low-grade zone of the Ryoke metamorphic belt in Japan. Color indices indicate a range of θ and ϕ values for this rock. It should be noted that we cannot distinguish the real azimuth, θ, from $\theta + 180°$. To obtain the unique *c*-axis orientation, an additional operation such as section tilting (Heilbronner and Pauli, 1993) or oblique light illumination (Wilson et al., 2007) is required. However, the data obtained by the Abrio imaging system alone are sufficient to determine crystal morphology and the angle between the *c*-axis and the vein wall (Fig. 2a). The angle between the *c*-axis and the plane of the vein wall (0–90°), γ (Fig. 2d), is a function of

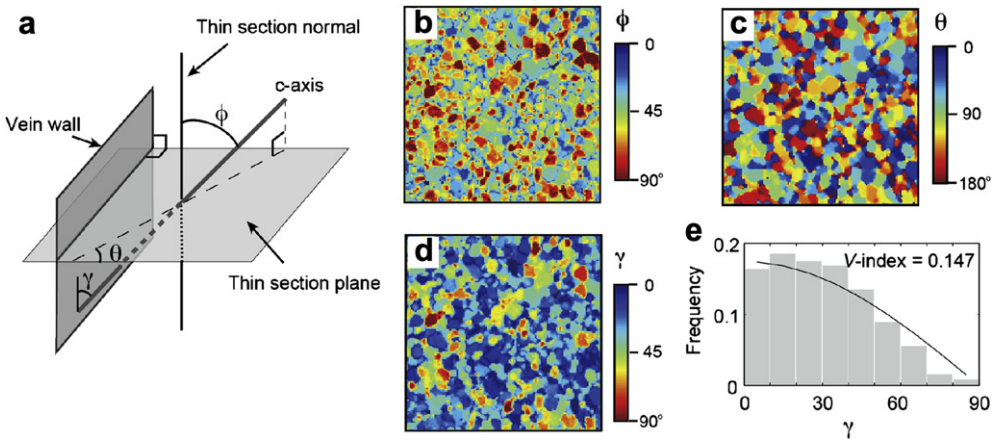

Fig. 2. (a) Schematic illustration of the system. The thin section was prepared normal to the vein wall. The *c*-axis orientation of quartz is defined by its azimuth, θ, and plunge, ϕ. The angle between the *c*-axis orientation and the vein wall plane, α, is a function of θ and ϕ. (b–d) Orientation images of a quartz aggregate in metachert (sample JU3-2CH) taken with the birefringence imaging system, showing the (b) plunge, ϕ (0–90°), (c) azimuth, θ (0–180°), and (d) *c*-axis orientation with respect to the vein wall, γ (0–90°). The images are 370.5 μm wide (150 pixels). The azimuth is the angle from the horizontal line in the images. (e) Histogram plot of γ. The black curve indicates the theoretical random distribution.

the azimuth, θ, and plunge, ϕ, because we prepared thin sections cut normal to the vein wall. We have derived the strength of the *c*-axis fabric intensity of quartz in a vein (*V*-index) relative to a random distribution, as follows:

$$V = \int |R_{\mathrm{rnd}}(\gamma) - R_{\mathrm{obs}}(\gamma)| d\gamma \tag{2}$$

A practical calculation is made for individual bins of a histogram:

$$V = \sum_{i=1}^{n} |R_{\mathrm{rnd,i}} - R_{\mathrm{obs,i}}| \cdot \frac{\pi}{n}, \tag{3}$$

where n is the number of bins, $R_{\mathrm{rnd,i}}$ is the theoretical distribution of γ for a random fabric, and $R_{\mathrm{obs,i}}$ is the observed distribution of γ (normalized using a number of data points). In the theoretical distribution of γ for a random fabric, the probability between the angles γ_1 and γ_2 ($\gamma_1 < \gamma_2$) is calculated as follows (Bloss, 1957):

$$R_{\mathrm{rnd}} = \cos(90^\circ - \gamma_1) - \cos(90^\circ - \gamma_2) \tag{4}$$

In this study, the bin size is set to 10° ($n = 9$), where the *V*-index ranges from 0 (random fabric) to 1.67 (all *c*-axis orientations are normal to the vein wall).

Fig. 2e shows a histogram of *c*-axis orientations, γ, in a quartz aggregate in the host rock (sample JU3-2CH). The *c*-axis orientations in this sample are close to the theoretical random distribution, and the *V*-index is 0.147. The random *c*-axis fabric in this rock is consistent with the results of analyses of quartz fabric in low-grade metachert of the Ryoke metamorphic belt, as reported by Okudaira et al. (2010) based on backscatter electron analyses.

4. Textures of synthetic quartz veins

In the synthetic veins, the epitaxial growth of quartz grains occurred on pre-existing quartz grain surfaces on outer surfaces and in the slits (Fig. 3a). Generally, the growth increment in the slit is less than the growth that occurred on outer surfaces. Most of the fluid flow was in the outer vessel space, which likely accounts for the difference in growth rates. The boundaries between veins and host rocks are clearly observed from fluid inclusion trails (Fig. 3b). No silica polymorphs other than quartz are observed on rock blocks, except for minor chalcedony and opal-C in the high-Si region. Maximum grain height is about 1 mm, found in sample JU3-5SS (Fig. 3a and c). Sandstone (JU3-6SS, $M_{\mathrm{Qtz}} = 0.52$) and granite (JU4-7GR, $M_{\mathrm{Qtz}} = 0.32$) blocks are partially composed of minerals other than quartz (Fig. 3c and d). A small number of quartz grains that nucleated in fluid were deposited on other mineral surfaces in the sandstone sample (JU3-6SS), whereas no precipitates are found in the granite sample (JU4-7GR). The lack of nucleated quartz grains in the granite sample (JU4-7GR) is a consequence of the low-Si content of the solution (100–103 ppm; Table 1), as quartz nucleation is difficult in such low-Si solutions (Okamoto et al., 2010). In the slit, quartz grain growth occurred from both walls, and some large grains impinged on others growing from the opposite wall (Fig. 3a and e).

Fluid inclusions are aligned along host rock/vein boundaries in all samples (Fig. 3b, d and e). In samples JU4-4IK, JU4-5IH, and JU4-7Gr, abundant fluid inclusions occur within quartz grains in the veins. Euhedral quartz grains in these samples are commonly zoned, with a fluid-inclusion-rich core and a fluid-inclusion-poor rim (Fig. 3f); the outline of the core is similar to the outline of the euhedral crystal. Most of the fluid inclusions in the veins are spherical and are <10 μm in size, although some elongate inclusions are greater than 100 μm long (Fig. 3b). These elongate inclusions are oriented parallel to the long axis of the quartz grain.

4.1. Shape and c-axis orientation of individual quartz grains growing from the wall

Fig. 4 shows *c*-axis orientation images of quartz grains growing from the outer block surfaces into free space. In samples JU3-2CH (Fig. 4a, metachert), JU4-5IH (Fig. 4b, metachert), and JU3-6SS (Fig. 4c, sandstone), the lengths of the long axes of most vein quartz grains are 3–10 times greater than those in the host rock. Quartz grains are elongate and columnar in shape, commonly developing hexagonal prism faces $m = \{10\bar{1}0\}$, and two rhombohedron faces $r = \{10\bar{1}1\}$ and $z = \{01\bar{1}1\}$, where *m*, *r*, and *z* are shown in Fig. 4b. In contrast, quartz grains growing from granite (JU4-7Gr) do not develop columnar shapes (Fig. 4d), but instead develop hill-like forms. This is a consequence of host-rock grain size (798 μm) exceeding the size of the vein increment (300–350 μm).

The long axis and *c*-axis (azimuth) orientations in the thin section plane (with respect to the vein wall) were measured for "well-grown" grains with axial lengths more than three times greater than the host-rock grain size (Fig. 5a). Well-grown grains are commonly oriented subnormal to the vein wall. Although grain

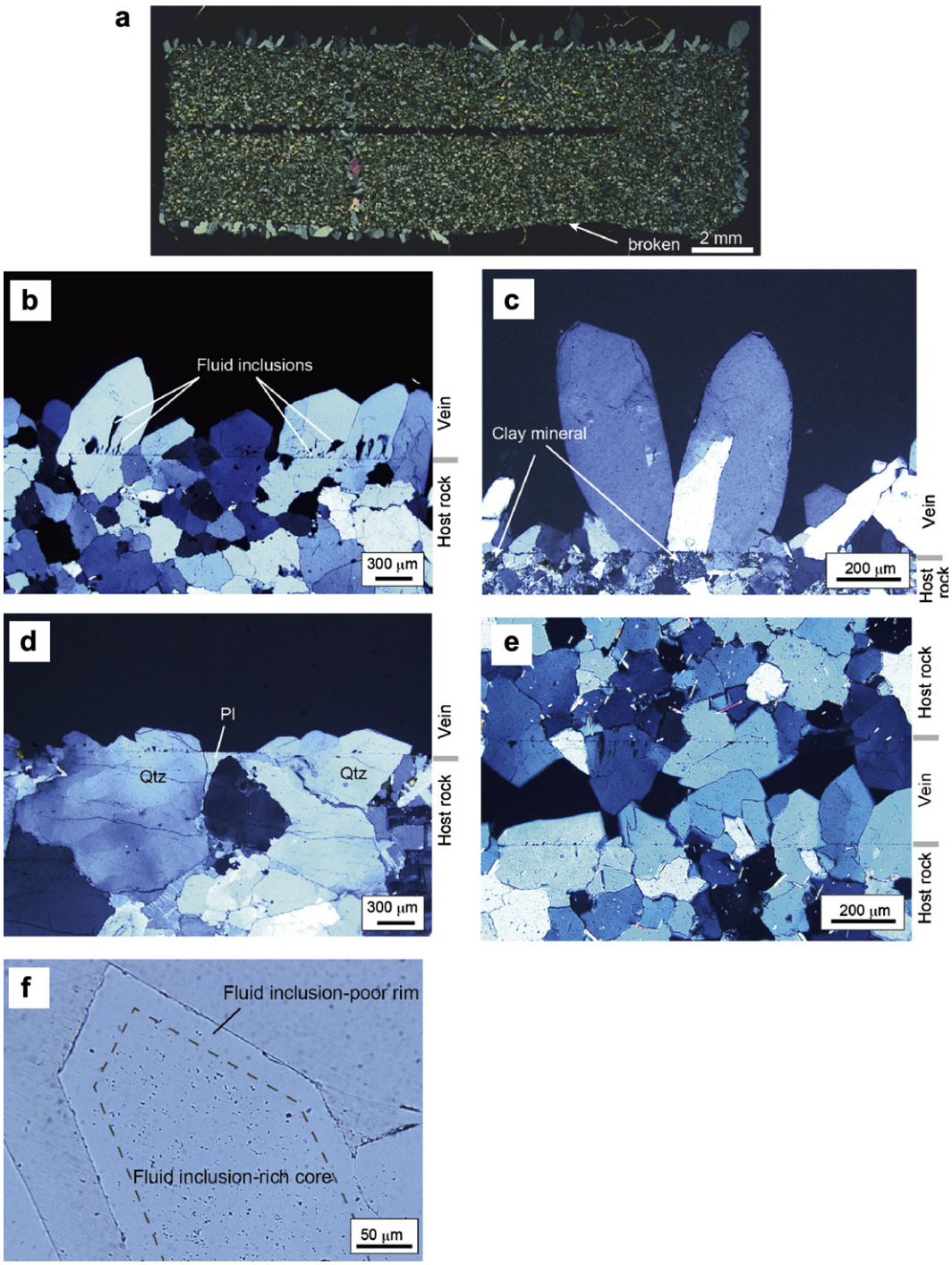

Fig. 3. (a–e) Photomicrographs, taken with a conventional optical microscope under crossed polarized light, of quartz crystals growing from the substrate surfaces. (a) An entire view of the sample JU3-6SS (sandstone). (b) JU4-4IK (metachert), (c) JU3-6SS (sandstone) and (d) JU4-7Gr (granite). (e) Photomicrograph of quartz crystals growing in a slit in sample JU4-4IK (metachert). (f) Photomicrograph (plane-polarized light) of quartz growing from the outer substrate surface of the sample JU4-5IH (metachert). Euhedral quartz crystals contain a fluid-inclusion-rich core and a fluid-inclusion-poor rim.

shape observed in thin section is also affected by the plunge of the grains (the angle with respect to the thin section plane), the orientation of the long axis is consistent with the *c*-axis orientation (Fig. 5a). This finding indicates that quartz grains preferred to grow parallel to the *c*-axis. For well-grown grains, the short axis increases in length from 20 to 400 μm as the long axis increases in length from 40 to 930 μm (Fig. 5b). The length of the short axis of a well-grown grain is defined as the maximum length in the direction normal to the long axis of the grain. In spite of variations in grain size among veins in different samples, the aspect ratio (long axis length/short axis length) of well-grown grains is similar in each case, ranging from almost 2 to 4 (average, ~2.9).

4.2. Textures of quartz aggregates growing from the outer surfaces of the rock blocks

During growth, quartz grains impinge on adjacent grains that have grown epitaxially on the adjacent host rock grains. Competitive

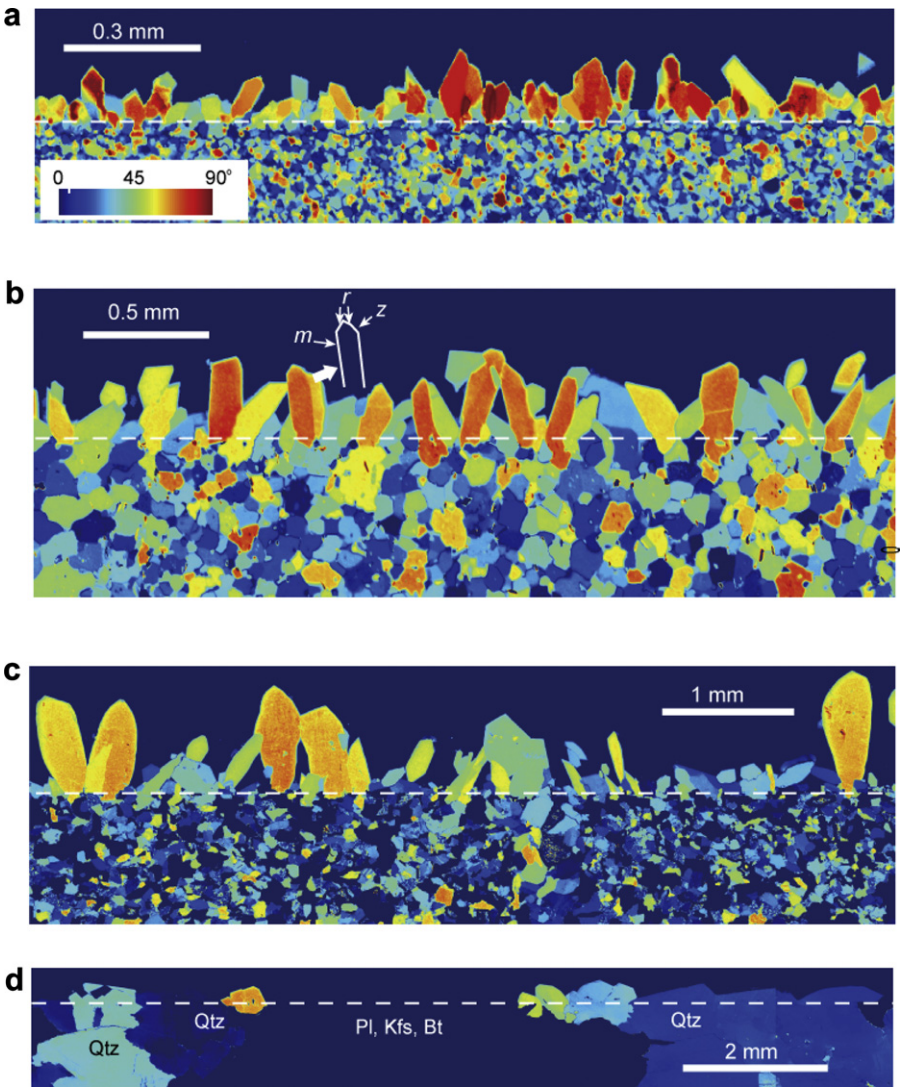

Fig. 4. *c*-axis orientation (the angle between the *c*-axis and the vein wall, γ) images of quartz crystals growing from the outer surface of the rock block in (a) JU3-2CH (metachert), (b) JU4-5IH (metachert), (c) JU3-6SS (sandstone), and (d) JU4-7Gr (granite). Minerals other than quartz in host rocks have a color index of $\gamma = 0$. The direction of fluid flow is from left to right, and the initial slit-wall surfaces are shown by dashed lines.

growth occurred reflecting the quartz *c*-axis orientations of the host rock grains. The degree of competitive growth was evaluated using the number of surviving grains (Fig. 6a) and the *V*-index (Fig. 6b), both with respect to the normalized distance from the vein wall, L/d, where L and d are the distance from the vein wall and the average crystal size in the host rock (d values are given in Table 1), respectively. The number of surviving grains was normalized using the number of quartz grains at the boundary between the vein and host rock ($L/d = 0$). In the normalized plot, the grain number profiles show a similar trend in four samples (Fig. 6a). The normalized grain number ranges from 0.8 to 1.2 in host rocks ($L/d < 0$). In veins, the grain number is similar to that of the host rock at sites near the wall, where L/d values are 0–1.6 for JU3-CH (metachert), 0–0.4 for JU4-5IH (metachert), 0–0.8 for JU4-4IK (metachert), and 0–1.2 for JU3-6SS (sandstone). In the sandstone sample (JU3-6SS), the number of grains increases slightly at $L/d = 0.6$, due to the incorporation of nucleated grains and grains growing into the thin section (Fig. 4c). In contrast, at distances from the wall with $L/d > \sim 1$, the number of grains clearly decreases with increasing distance. At the normalized distance of five, the normalized grain number reaches ~0.2. These results indicate that competitive growth did not occur at the initial stages of growth: it only became significant when the growth increments normal to the vein wall reached dimensions similar to the host-rock grain size ($L/d > \sim 1$). Hereafter, growth stages both without (1) and with (2) competitive growth are referred to as stages 1 and 2, respectively (Fig. 6a).

The *V*-index was obtained from pixels in individual lines oriented parallel to the vein wall. The *V*-index changes systematically with distance from vein wall (Fig. 6b). In the host rock, *V*-index values are less than 0.5 (Figs. 2e and 6b), indicating that the *c*-axis orientation of quartz in the host rock has a nearly random distribution. For veins close to the wall (stage 1, $L/d = 0$–1) in samples JU3-2Ch (metachert), JU4-5IH (metachert), and JU3-6SS (sandstone), values of the *V*-index are nearly constant. Although the *V*-index shows an immediate increase from the vein wall in sample JU4-4IK (metachert), the *V*-index value at a site located close to the vein wall ($L/d = 0.3$) is within the range of values in the host rock (*V*-index = 0.2–0.5). In stage 2, the *V*-index increases with increasing L/d from 1 to 4. This result suggests that a concentration of the *c*-axis fabric (i.e., the deviation from the random distribution) occurred during competitive growth. The trend in the *V*-index is most evident for the fine-grained metachert sample (JU3-2CH),

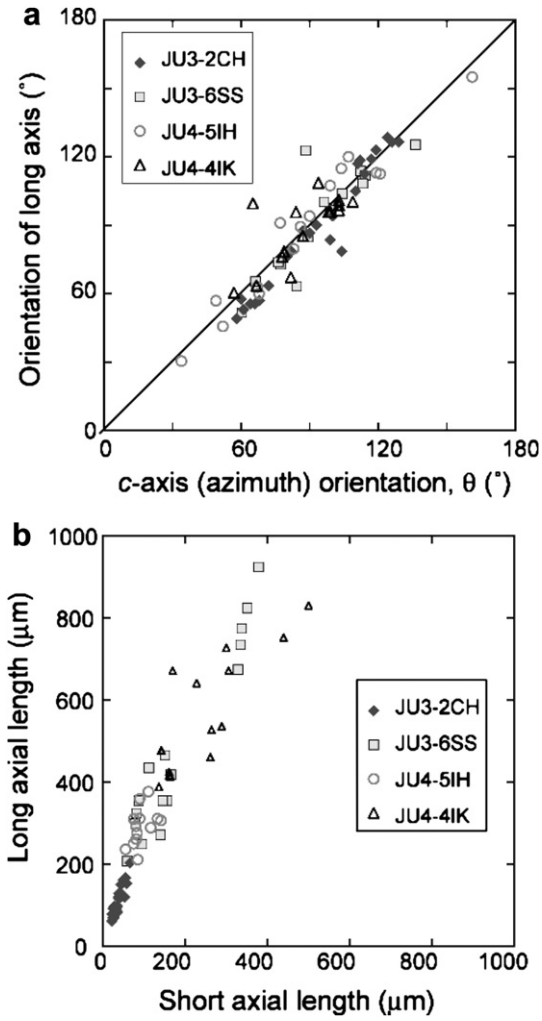

Fig. 5. (a) Orientation of the long axis in the thin-section plane versus the azimuth of the *c*-axis for well-grown quartz crystals. (b) Length of the long axis versus length of the short axis for well-grown quartz crystals.

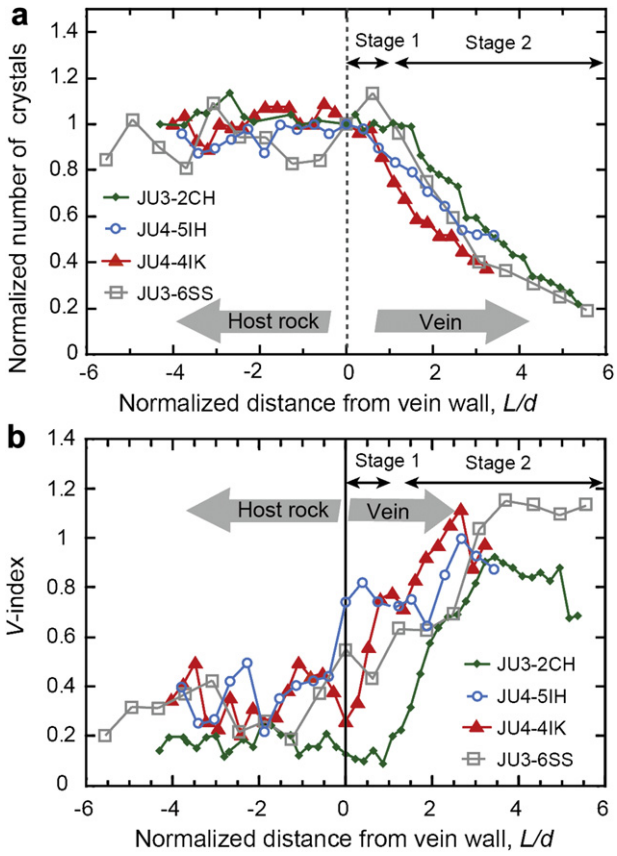

Fig. 6. Features of competitive growth in relation to distance from the vein wall (for growth into an open cavity). The distance from the vein wall, *L*, is normalized by the average crystal size in the host rock, *d* (Table 1). The vein/host rock boundary is set to zero. (a) Number of surviving crystals normalized by the number of crystals at the vein/host rock boundary, n_0. (b) *V*-index, obtained from pixels in lines oriented parallel to the vein wall. Competitive growth is absent near the wall (L/d = 0–1; stage 1), whereas it is significant at sites further from the wall (L/d > ~1; stage 2).

which contains many grains in the analyzed area (Fig. 6a). This concentration of quartz aggregate *c*-axis fabrics is similar to that found in natural elongate–blocky veins (Cox and Etheridge, 1983; Nüchter and Stöckhert, 2007).

The change in individual crystal morphology from hill-like to columnar (as described above) corresponds to the change from stage 1–2. We emphasize that the critical factor for this transition is not the absolute height of the crystal growth increment, but the ratio of growth increment to host-rock grain size. Fig. 6 does not show data for the granite sample JU4-7Gr (Figs. 3c and 5d) because of the very small number of grains. In sample JU4-7Gr, the maximum height of grains is 499 μm (L/d = 0.6). Grains show evidence of stage 1 growth and competitive growth did not occur for L/d values from 0 to 0.6, which is consistent with the results obtained for the other samples (Fig. 6).

4.3. Textures of quartz aggregates growing in the slit

The nature of polycrystal growth from adjacent walls is similar to growth on the outer surfaces until grain impingement occurs (Fig. 7). A systematic decrease in growth in the direction of flow is not observed. Instead, heterogeneity of crystal sizes was produced in the slit, which is dependent on the *c*-axis orientation and the presence of quartz grains on the slit wall.

The slit aperture, *H*, is similar among samples (H = 304–353 μm), whereas host-rock grain size is highly variable (d = 23–798 μm) (Table 1). Vein textures change depending on the normalized slit aperture value, H/d. In fine-grained metachert (JU3-2CH, H/d = 13.8), the slit aperture is large enough for quartz aggregates to have reached the stage of competitive growth (stage 2) (Fig. 7a). In contrast, quartz grains in the slit of granite blocks (JU4-7Gr, H/d = 0.4) grew in a direction normal to the slit wall, without significant thickening (white arrows in Fig. 7b). These crystals would impinge on one other while still at stage 1. In samples JU4-6SS (sandstone; H/d = 4.8; Fig. 7c) and JU4-4IK (metachert; H/d = 2.4; Fig. 7d), some crystals impinge on one other yet do not produce crystals that bridge the vein. This occurs because grains on both sides have different crystallographic orientations, due to the slit being larger than the grain size in the host rock (Table 1). Concavo-convex grain boundaries develop at sites of grain impingements (Figs. 3e and 7d).

5. Discussion

5.1. Morphological evolution of a single crystal growing from a wall

A two-dimensional crystal growth model is useful in terms of understanding the morphological changes of individual grains and

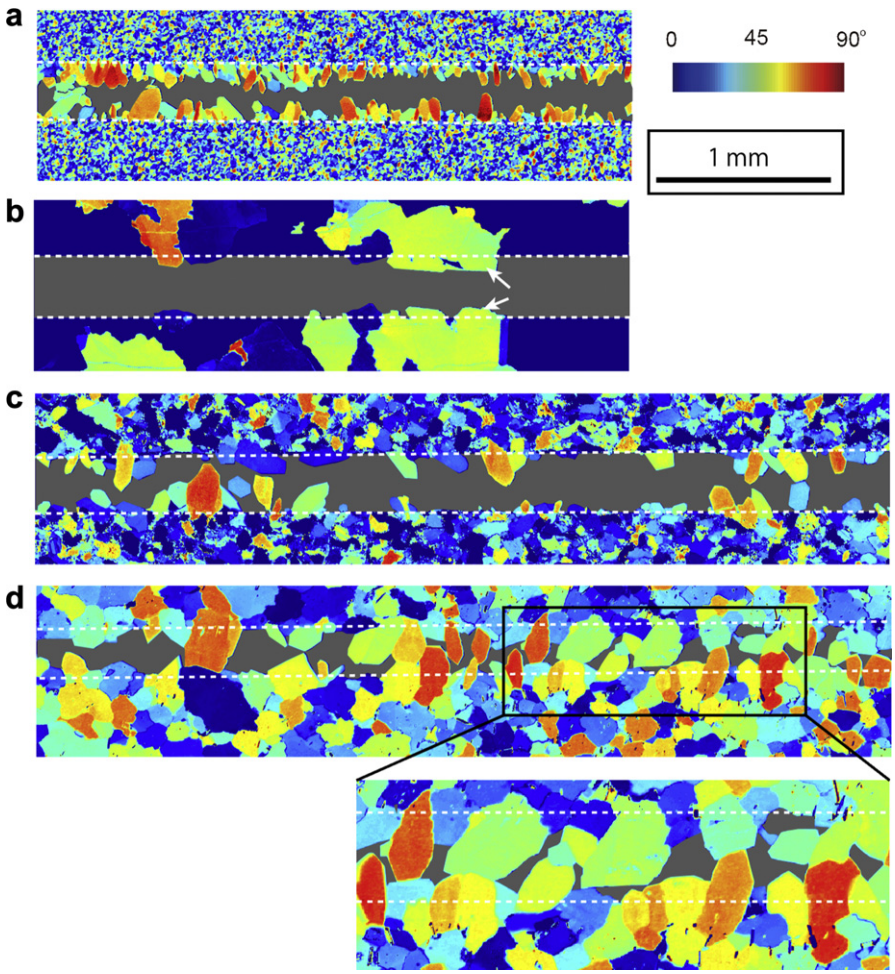

Fig. 7. *c*-axis orientation (the angle between the *c*-axis and the vein wall, γ) images of quartz crystals growing in the slit in (a) JU3-2CH (metachert), (b) JU4-7Gr (granite), (c) JU3-6SS (sandstone), and (d) JU4-4IK (metachert). Fig. 7d includes a high-magnification view to show the concavo-convex grain boundary. The direction of fluid flow is from left to right. The vein/host rock boundaries are shown by dashed lines, and the pore spaces in the slits are shaded gray. Minerals other than quartz in host rocks have a color index of $\gamma = 0$. In Fig. 7b, white arrows indicate crystals with the same crystallographic orientation, located adjacent to one another on opposing walls.

the development of textures of syntaxial quartz veins that were observed in the synthetic quartz veins. The fundamental algorithm used in our study is after the *Vein Growth* program developed by Bons (2001), Hilgers et al. (2001), and Nollet et al. (2005). In the model, grains are defined by nodes that are linked by short straight lines, and grain growth into the open fracture is simulated by the movement of these nodes in many small increments. The time from the beginning of grain growth is defined by the number of growth steps, which is the number of repeated operations with small increments. The morphology of individual quartz crystals is controlled by the anisotropic growth rate of crystal faces, which is in the following order: *c* face (basal) > *r*, and *z* face (rhombohedron) > *m* face (prism) (e.g. Ostapenko and Mitsyuk, 2006). For simplicity, quartz morphology is assumed to be prismatic, with *m* and *r* faces. The relative growth rate is a function of the angle between the *c*-axis and the pole normal to the quartz surface (Bons, 2001), as shown in Fig. 8a; growth is fastest in the *c*-axis direction, and is slowest normal to the *c*-axis. The growth rate has a local minimum at an angle of 30° relative to *c*-axis direction. Growth produces a columnar crystal with an aspect ratio of ~5.4, and when halved, is similar to the aspect ratio of quartz grains in synthetic veins (~2.9; Fig. 5b).

In this section, we consider the growth of a single crystal from a substrate crystal (Fig. 8b and c). The substrate crystal has a flat surface, with the *c*-axis oriented normal to the vein wall. The aspect ratio of a crystal is defined as height/width, where height and width are the maximum lengths of the crystal in directions normal and parallel to the wall, respectively (Fig. 8d). Using this definition, the aspect ratio is less than 1.0 initially, when the crystal height is significantly less than the width of the substrate quartz. The morphological change from growth stage 1–2 is reproduced by this model. At a growth step of less than ~1000 in the model (Fig. 8c), crystal growth is normal to the vein wall, without significant widening, resulting in a considerable increase in the aspect ratio to 2.2. At this stage, crystal facets do not fully develop. Grain morphology at this stage corresponds to stage 1 growth in synthetic veins, where crystal height is less than the host-rock grain size (Figs. 3d, 4d and 7b). When the growth step exceeds ~1000, crystal growth continues with a similar morphology, and width increases with increasing height (Fig. 8c). The morphology of grains at this stage corresponds to the euhedral grain morphology in synthetic veins at stage 2, where grain height is greater than the grain size in the host rock (Figs 3b, 4a–c). The growth of euhedral crystals in the model (Fig. 8c) is supported by the euhedral outline of the fluid-inclusion-rich core in quartz crystals within the veins (Fig. 3f). The transition from stage 1–2 occurs gradually, with the aspect ratio shifting toward a steady state value of 2.7 (Fig. 8c). The steady state value of the aspect ratio in the 2D crystal growth model

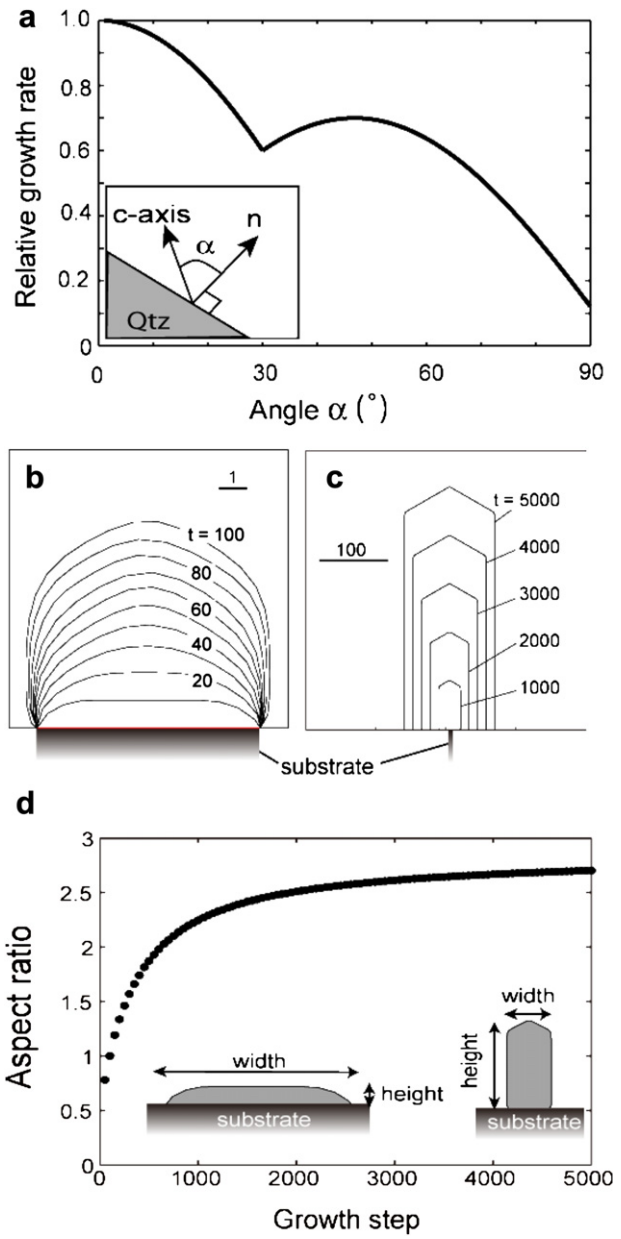

Fig. 8. Two-dimensional crystal growth model using the algorithm from *Vein Growth* (Bons, 2001). (a) Growth rate function for the prismatic mineral used in the numerical simulation of two-dimensional growth. (b, c) The evolution of morphology during single-crystal growth (the *c*-axis is normal to the vein wall) at (b) 100 time steps and (c) 5000 time steps. (d) Evolution of the aspect ratio (= height/width) with time for single-crystal growth.

(2.7, Fig. 8c) is slightly different from that observed in the synthetic veins (~2.9, Fig. 5b); however, the 2D crystal growth model well reproduces the morphological evolution of quartz crystals in the synthetic veins. Although we did not perform the numerical simulation of polycrystal growth, it is clear that the grain widening at stage 2 causes the impingement of adjacent crystals and competitive growth. Nollet et al. (2005) showed that the hybrid 2D-growth algorithm for irrational growth (*Vein Growth*, Bons, 2001) and faceted growth (*Facet*, Zhang and Adams, 2002) is important to effectively model the nature of the competitive growth in a free space. The two growth stages observed in our synthetic veins are qualitatively similar to those in the simulation. More detailed comparison between synthetic veins and numerical simulations will provide a quantitative basis on the model of vein formation.

Based on a two-dimensional simulation (using *Vein Growth*), Hilgers et al. (2001) reported the critical distance for the onset of competitive growth to be 10 μm. This value is true for most crustal rocks, because grain size is commonly larger than several tens of microns. However, the results of the present study suggest that the critical distance is not unique, and should instead be defined as the ratio of normalized distance to host-rock grain size, L/d. The critical value of this ratio, for the onset of competitive growth, is $L/d = \sim 1$ (Fig. 6).

5.2. Comparison with natural veins

Fig. 9 shows veins from the Shimanto accretionary complex in the Muroto area, Japan. These veins are hosted by sandstone that forms part of sample JU4-6SS, and are composed mainly of quartz, with minor calcite. Thick veins (width = 4.6 mm) exhibit elongate–blocky textures, characterized by quartz crystal growth on both vein walls, and by large grains with *c*-axis orientations subnormal to the vein wall (Fig. 9a). At the quartz/calcite interface, crystal facets developed in quartz. The vein *V*-index increases symmetrically from ~0.25 to ~1.0 with increasing the distance from the

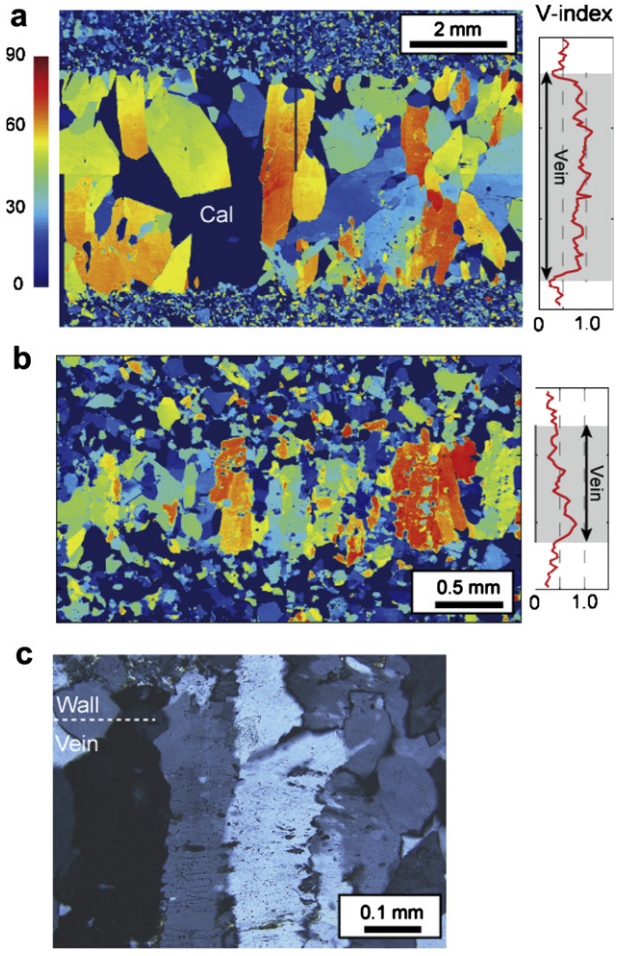

Fig. 9. Quartz vein textures in samples from the Shimanto accretionary complex, Japan. (a, b) *c*-axis orientation (γ) image and *V*-index profile of (a) a thick elongate–blocky vein (4.6 mm in width) and (b) a thin vein composed of elongate crystals that bridge the vein (0.8 mm in width). Minerals other than quartz are shown with a color index of $\gamma = 0$. Cal = calcite. (c) Optical microphotograph of elongate crystals that bridge the vein. Crystal fibers show serrated grain boundaries and contain multiple trails of fluid and host-rock inclusions, indicating the occurrence of crack–seal events.

vein walls. These features are consistent with those observed in synthetic veins that formed in open cavities (Figs. 4c and 6c). In contrast, thin veins (width = 0.8 mm) are composed of elongate crystals that bridge the veins (Fig. 9b). The long axes of crystal bridges are oriented normal to the vein wall, regardless of *c*-axis orientation, and the vein *V*-index does not increase. These features indicate the absence of competitive growth. Thin veins have serrated grain boundaries and fluid inclusion bands at intervals of 5–50 μm (Fig. 9c), similar to commonly observed stretched crystal veins (e.g. Stowell et al., 1999; Okamoto et al., 2008). However, it is difficult to determine whether the texture of the thin vein was produced by ataxial (stretched crystal texture) or syntaxial vein growth (fibrous texture), based solely on optical observations. The experiments performed in this study did not produce the texture observed in the thin vein (elongate crystal bridges without competitive growth; Fig. 9b). Therefore, the following question remains: What controls the development of textures with and without competitive growth and the formation of crystal bridges during vein growth?

In a crack with no shear displacement, quartz fragments have the same crystallographic orientation on both sides of the vein wall (Fig. 10). We consider biaxial growth in thick ($H/d = 10$; Fig. 10a and b) and thin ($H/d = 0.4$; Fig. 10c and d) cracks. The growth model is the same as that used for Fig. 8. In a thick crack, facet development occurs during quartz growth (stage 2), and the long axis is oriented parallel to the *c*-axis (Fig. 10a and b). Some grains, with their *c*-axis oriented normal to the vein wall, readily impinge on each other, producing crystals that bridge the crack (Fig. 10a). However, the *c*-axis orientation usually deviates from being normal to the vein wall. As a result, the main growth directions for grains on opposing walls are inclined with respect to each other, making it difficult for such grains to impinge on one another without significant widening of the grain relative to the host rock grain size (Fig. 10b). This results in the development of elongate–blocky textures, as observed in synthetic veins hosted by fine-grained metachert ($H/d = 13.2$; Fig. 7a) and in natural veins ($H/d = 60$; Fig. 9a).

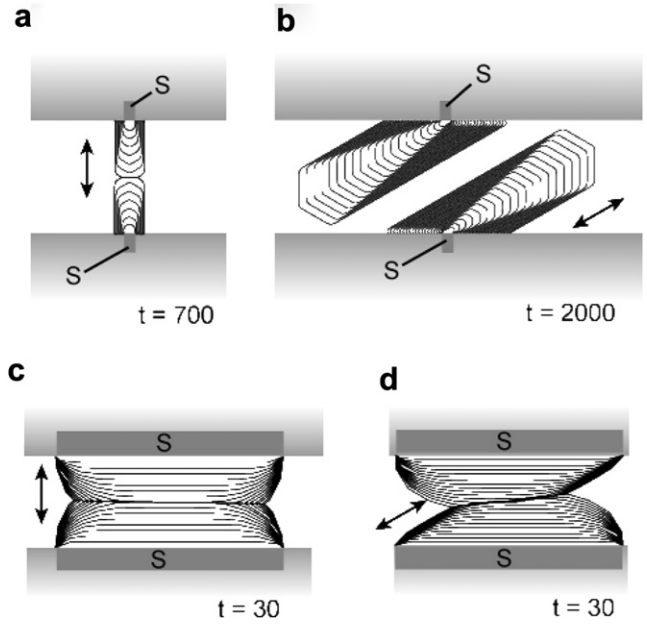

Fig. 10. Two-dimensional crystal growth in a crack, simulated by the same model as that described in Fig. 8. Substrate grains, labeled as *S*, on both sides of the vein wall have the same *c*-axis orientation, indicated by arrows. Four cases were simulated with different crack aperture, *H*, relative to host-rock grain size, *d*, and different *c*-axis orientation from vein walls, θ. *t* indicates the time steps. (a) $H/d = 10$, $\theta = 90^\circ$, (b) $H/d = 10$, $\theta = 30^\circ$, (c) $H/d = 0.4$, $\theta = 90^\circ$ and (d) $H/d = 0.4$, $\theta = 30^\circ$.

In a thin crack, grains from the opposing walls impinge on one another at stage 1 (Fig. 10c and d), producing crystal bridges over the crack. During impingement, grain width does not increase significantly. In addition, grains in which the *c*-axis is oriented normal to the vein wall (Fig. 10c) and those in which the *c*-axis is oriented at 30° to the vein wall (Fig. 10d) impinge at approximately same time (Fig. 10d). This result suggests that the growth rate is isotropic at stage 1. Similar features are observed for grain growth in the granite slit (JU4-7Gr; $H/d = 0.4$; white arrows in Fig. 7b), although grains have not yet impinged on one another.

We note that the width of the thin vein composed of crystal bridges ($H/d = 10$; Fig. 9b) does not represent the width of the crack aperture, but rather the integrated width of numerous crack–seal events. When the spacing of fluid inclusion bands is taken as the width of individual crack apertures (Fig. 9c), the value of H/d is 0.06–0.63, which is consistent with the scenario shown in Fig. 10c and d. Serrated grain boundaries between adjacent crystal fibers are interpreted to develop as cusps at the site of grain impingement (Fig. 10c and d). Such a cusp will be filled by adjacent crystals, which grow faster (Becker et al., 2011). When the formation and sealing of such thin cracks occur repeatedly at different sites in a vein, a stretched crystal texture is developed. Similarly, the vein width of elongate–blocky veins does not always reflect the real crack aperture from a single crack–seal event. When progressive widening occurs during sealing, high-H/d cracks indicate that the rate of crack opening exceeds the growth rate (Hilgers et al., 2001). Hilgers et al. (2001) also suggested that the roughness of the vein wall is critical for competitive growth. We cannot address this effect, because we used a substrate with a flat surface. Additional experiments with realistic fractures are required to fully understand the process of vein formation.

5.3. Evolution of fracture porosity during crack–sealing

Common crustal rocks are not monomineralic and contain quartz grains with variable *c*-axis orientations. The results of this study suggest that during the formation of a syntaxial vein, grain-scale heterogeneity in a crack is developed depending on the size and the *c*-axis orientations of grains in the host rock. The evolution of fracture porosity during sealing depends on the modal abundance, spatial distribution, and *c*-axis orientation of quartz in the vein wall.

The generation of heterogeneous structures of fracture porosity plays an important role in the formation of lenticular veins. When we consider crack–sealing via mineral deposition from supersaturated solutions in a single flow path, mineral deposition occurs preferentially near the inlet, because the degree of supersaturation is decreased by precipitation (Lee et al., 1996; Lee and Morse, 1999; Hilgers et al., 2004; Okamoto et al., 2010). This deposition can result in plugging of the crack close to the fluid inlet, making it difficult to form a mineral vein with a lenticular shape. Lee et al. (1996) pointed out that for a lenticular crack to seal uniformly, either an extremely high flow rate or low supersaturation is required. Conversely, in the present study, quartz growth in the slit was fairly uniform in the direction of flow (Figs. 3a and 8). Even when grains had both favorable orientation and impingement at favorable sites, fractures did not seal completely because some pore spaces are surrounded by the slow-growing *m* faces of quartz. In addition, sites in contact with host rock minerals other than quartz were not sealed. The development of 3D connectivity between such sites could create a flow path. Similar phenomena have been reported for the *in situ* growth of polycrystalline alum (Hilgers and Urai, 2002b), in which growth was observed to have continued after impingement of a few grains near the inlet. Heterogeneous structures of fracture porosity may potentially produce a tortuous

channel flow in the crack plane (Watanabe et al., 2008), which would affect the sites of subsequent crystallization. The detailed pattern of grain growth can be used to understand the evolution of the fluid pathway in a crack. The growth pattern can be determined using cathodoluminescence and/or by examining lateral variations in fluid inclusion compositions.

The sealing of cracks and faults is closely associated with the evolution of fluid pressure and with the earthquake cycle (Sibson, 1990, 2009). After rupturing, mineral deposition in cracks lowers the permeability and re-establishes rock strength (Tenthorey and Cox, 2006). The mechanical and hydrological behavior of individual cracks is dependent on the evolution of the fracture porosity during sealing. An extensional crack is opened in response to a rise in pore fluid pressure, and collapses when pore fluid pressure decreases as fluid drains (e.g. Etheridge et al., 1984; Hilgers and Urai, 2002a). The observations of synthetic quartz vein formation indicate that rates of sealing in the direction of the crack opening are highly variable due to the anisotropy in growth rate (Fig. 7). Once the fastest-growing grains impinge on the opposite wall, they can prop the crack open, even if fluid pressure decreases (e.g. Fisher and Brantley, 1992; Gale et al., 2010; Laubach et al., 2004). In contrast, a much longer time is needed to seal pore spaces between fast-growing crystals; i.e., those spaces surrounded by host-rock minerals other than quartz, or by quartz facets with slow-growing orientations. In the Shimanto veins, spaces filled by calcite (Fig. 9a) could reflect later-stage sealing of relict open pore spaces. Such structures (incompletely sealed cracks) also have been reported in sedimentary rocks (e.g. Laubach et al., 2004; Gale et al., 2010), and may be abundant in the upper crust. As such, and on the basis of our study, we suggest that incompletely sealed cracks with spatially variable porosity may be important fluid pathways and planes of weakness in the upper crust.

6. Conclusions

Syntaxial quartz veins were synthesized by hydrothermal flow-through experiments at 430 °C and 31 MPa using rock substrates (metachert, sandstone, and granite) containing slits. The textures (grain shape, size, *c*-axis orientation, long axis orientation, etc.) of the produced synthetic veins were analyzed by birefringence imaging microscopy, providing information on the development of natural vein textures and the evolution of fracture porosity during crack–sealing, as follows:

1. In terms of crystal morphology, the growth of quartz from the wall into an open cavity was divided into two stages. During stage 1, quartz grain growth was normal to the substrate, grain width did not increase, and crystal facets did not develop. During stage 2, quartz grains developed facets and grew preferentially parallel to the *c*-axis. The aspect ratio of quartz grains shifted toward a steady state value of ~2.9 in our experiments. At this stage, the orientation of the long axis of the quartz grain was consistent with its *c*-axis orientation.
2. Competitive growth among adjacent grains occurred during the stage 2, which was characterized by a concentration of quartz *c*-axes normal to the vein wall. The transition from stage 1 to stage 2, with respect to distance from the vein wall, depends on the grain size of quartz in the substrate.
3. The textures of syntaxial veins with and without competitive growth result from the impingement of grains from both sides of the vein at stages 1 and 2, respectively. The nature of the texture that develops depends on the size of the crack aperture, *H*, relative to the grain size of quartz in the host rock, *d*. In cracks with a high *H*/*d* value, quartz grains on both sides impinge on one another during growth stage 2, producing elongate–blocky veins. In cracks with a low *H*/*d* value, quartz grains on both sides impinge on one another during growth stage 1, producing crystals that bridge the crack without competitive growth. When the formation and sealing of such thin cracks occur repeatedly at different sites in a vein, stretched crystal texture is developed.
4. Heterogeneous structures of fracture porosity develop during syntaxial vein growth, depending on grain size, crystallographic orientation, and modal abundances of quartz in the vein wall. When growing quartz grains impinge on grains growing from the opposite vein wall, they form crystal bridges and can prop open cracks. Such incompletely sealed cracks may exist in abundance in the upper crust, acting as important fluid pathways and planes of weakness.

Acknowledgments

We appreciate T. Okudaira, T. Masuda, and Y. Omori for kindly providing the metachert samples used in the experiments. We are grateful to N. Tsuchiya and H. Saishu for valuable discussions. Constructive reviews by S.F. Cox and K. Van Noten and careful editorial handling by T.G. Blenkinsop are greatly appreciated. This study was supported by a Grant-in-Aid for Scientific Research on Innovative Areas to A. Okamoto (No. 22109501) from the Ministry of Education, Culture, Sports, Science and Technology of Japan, and to K. Sekine (No. 21686083) from the Japan Society for the Promotion of Science.

References

Becker, S., Hilgers, C., Kukla, P.A., Urai, J.L., 2011. Crack-seal microstructure in bimineralic quartz-chlorite veins in shales and siltstones from the RWTH-1 well, Aachen, Germany. Journal of Structural Geology 33, 676–689.
Bloss, F.D., 1957. Anisotropy of fracture in quartz. American Journal of Science 255, 214–235.
Bons, P.D., 2000. The formation of veins and their microstructures. In: Jessell, M.W., Urai, J.L. (Eds.), Stress, Strain and Structure. A Volume in Honour of W.D. Means, vol. 2. Journal Virtual Explore.
Bons, P.D., 2001. Development of crystal morphology during uniaxial growth in a progressively widening vein: I. The numerical model. Journal of Structural Geology 23, 865–872.
Cox, S.F., Etheridge, M.A., 1983. Crack-seal fibre growth mechanism and their significance in the development of oriented layer silicate microstructures. Journal of Structural Geology 92, 147–170.
Etheridge, M.A., Wall, V.J., Cox, S.F., 1984. High fluid pressure during regional metamorphism and deformation: implications for mass transport and deformation mechanisms. Journal of Geophysical Research 89, 4344–4358.
Fisher, D.M., Brantley, S.L., 1992. Models of quartz overgrowth and vein formation: deformation and episodic fluid flow in an ancient subduction zone. Journal of Geophysical Research 97, 20043–20061.
Fournier, R.O., Potter, R.W.I.I., 1982. An equation correlating the solubility of quartz in water from 25 to 900 °C up to 10,000 bars. Geochimica et Cosmochimica Acta 46, 1969–1973.
Fueten, F., Goodchild, J.S., 2001. Quartz c-axes orientation determination using the rotating polarizer microscope. Journal of Structural Geology 23, 895–902.
Gale, J.F.W., Lander, R.H., Reed, R.M., Laubach, S.E., 2010. Modeling fracture porosity evolution in dolostone. Journal of Structural Geology 32, 1201–1211.
Heilbronner, R.P., Pauli, C., 1993. Integrated spatial and orientation analysis of quartz c-axes by computer-aided microscopy. Journal of Structural Geology 15, 369–382.
Heilbronner, R.P., Tullis, J., 2006. Evolution of c axis pole figures and grain size during dynamic recryllization: results from experimentally sheared quartzite. Journal of Geophysical Research 111, B10202. doi:10.1029/2005JB004194.
Hilgers, C., Koehn, D., Bons, P.D., Urai, J.L., 2001. Development of crystal morphology during uniaxial growth in a progressively widening vein: II. Numerical simulations of the evolution of anitaxial fibrous veins. Journal of Structural Geology 23, 873–885.
Hilgers, C., Urai, J.L., 2002a. Microstructural observations on natural syntectonic fibrous veins: implications for the growth process. Tectonophysics 352, 27–274.
Hilgers, C., Urai, J.L., 2002b. Experimental study of syntaxial vein growth during lateral fluid flow in transmitted light: first results. Journal of Structural Geology 24, 1029–1043.
Hilgers, C., Dilg-Gruschinski, K., Urai, J.L., 2004. Microstructural evolution of syntaxial veins formed by advective flow. Geology 32, 261–264.
Hilgers, C., Tenthorey, E., 2004. Fracture sealing of quartzite under a temperature gradient: experimental results. Terra Nova 16, 173–176.

Lee, Y.-J., Morse, J.W., Wiltscko, D.V., 1996. An experimentally verified model for calcite precipitation in veins. Chemical Geology 130, 203–215.
Lee, Y.-J., Morse, J.W., 1999. Calcite precipitation in synthetic veins: implication for the time and fluid volume necessary for vein filling. Chemical Geology 156, 151–170.
Laubach, S.E., Reed, R.M., Olson, J.E., Lander, R.H., Bonnell, L.M., 2004. Coevaluation of crack-seal texture and fracture porosity in sedimentary rocks: cathodoluminescence observations of regional fractures. Journal of Structural Geology 26, 967–982.
Nollet, S., Urai, J.L., Bons, P.D., Hilgers, C., 2005. Numerical simulations of polycrystal growth in veins. Journal of Structural Geology 27, 217–230.
Nollet, S., Hilgers, C., Urai, J.L., 2006. Experimental study of polycrystal growth from an advecting supersaturated fluid in a model fracture. Geofluids 6, 185–200.
Nüchter, J.-A., Stöckhert, B., 2007. Vein quartz microfabrics indicating progressive evolution of fractures into cavities during postseismic creep in the middle crust. Journal of Structural Geology 29, 1445–1462.
Okamoto, A., Kikuchi, T., Tsuchiya, N., 2008. Mineral distribution within polymineralic veins in the Sanbagawa belt, Japan: implications for mass transfer during vein formation. Contributions to Mineralogy and Petrology 156, 323–336.
Okamoto, A., Tsuchiya, N., 2009. Velocity of vertical fluid ascent within vein-forming fractures. Geology 37, 563–566.
Okamoto, A., Saishu, H., Hirano, N., Tsuchiya, N., 2010. Mineralogical textural variation in hydrothermal flow-through experiments: implications for quartz vein formation. Geochimica Cosmochimica Acta 74, 3692–3706.
Okudaira, T., Ogawa, D., Michibayashi, K., 2010. Grain-size-sensitive deformation of upper greenschist- to lower amphibolite-facies metacherts from a low-*P* metamorphic accretionary complex. Tectonophysics 492, 141–149.
Oliver, N., Bons, P., 2001. Mechanisms of fluid flow and fluid–rock interaction in fossil metamorphic hydrothermal systems inferred from vein–wallrock patterns, geometry and microstructure. Geofluids 1, 137–162.
Ostapenko, G.T., Mitsyuk, B.M., 2006. Asymmetry of growth and dissolution on basal, minor rhombohedral and prism faces of quartz. Journal of Crystal Growth 294, 330–338.
Passchier, C.W., Trouw, R.A.J., 2005. Microtectonics, second ed. Springer-Verlag, Berlin, p. 366.
Ramsay, J.G., Huber, M.I., 1987. The Techniques of Modern Structural Geology. In: Folds and Fractures, vol. 2. Academic Press, London.
Sander, B., 1950. Einfhürung in die Gefügekunde der geologiscen Körper. Springer, Berlin, p 399.
Sekine, K., Okamoto, A., Hayashi, K., 2011. In situ observation of the crystallization pressure induced by halite crystal growth in a microfluidic channel. American Mineralogist 96, 1012–1019.
Shribak, M., Oldenbourg, R., 2003. Techniques for fast and sensitive measurements of two-dimensional birefringence distributions. Applied Optics 42, 3009–3017.
Sibson, R.H., 1990. Conditions for fault-valve behavior. In: Knipe, R.J., Rutter, E.H. (Eds.), Deformation Mechanisms, Rheology and Tectonics. Geological Society Special Publication, vol. 54, pp. 15–28.
Sibson, R.H., 2009. Rupturing in overpressured crust during compressional inversion-the case from NE Honshu, Japan. Tectonophysics 473, 404–416.
Stowell, J.F.W., Watson, A.P., Hudson, N.F.C., 1999. Geometry and populations systematics of a quartz vein set, Holy Island, Anglesey, North Wales. In: McCaffrey, K.J.W., Lonergan, L., Wilkinson, J.J. (Eds.), Fractures, Fluid Flow and Mineralisation. Geological Society, London, Special Publications, vol. 155, pp. 17–33.
Tenthorey, E., Cox, S.F., 2006. Cohesive strengthing of fault zones during the interseismic period: an experimental study. Journal of Geophysical Research 111, B09202. doi:10.1029/2005JB004122.
Urai, J.L., Williams, P.F., van Roemund, H.L.M., 1991. Kinematics of crystal growth in syntectonic fibrous veins. Journal of Structural Geology 13, 823–836.
Van Noten, K., Muchez, P., Sintubin, M., 2011. Stress-state evolution of the brittle upper crust during compressional tectonic inversion as defined by successive quartz vein types (High-Ardenne slate belt, Germany). Journal of the Geological Society, London 168, 407–422.
Watanabe, N., Hirano, N., Tsuchiya, N., 2008. Determination of aperture structure and fluid flow in a rock fracture by high-resolution numerical modeling on the basis of a flow-through experiment under confining pressure. Water Resource Research 44, W06412. doi:10.1029/2006WR005411.
Wilson, C.J.L., Russell, D.S., Kunze, K., 2007. The analysis of quartz *c*-axis fabric using a modified optical microscope. Journal of Microscopy 227, 30–41.
Wilson, C.J.L., Robinson, J.A., Dugdale, A.L., 2009. Quartz vein fabrics coupled to elevated fluid pressures in the Stawell gold deposit, south-eastern Australia. Mineralium Deposita 44, 245–263.
Zhang, J., Adams, J.B., 2002. FACET: a novel model of simulation and visualization of polycrystalline thin film growth. Modeling and Simulation in Mineral Science and Engineering 10, 381–401.